Multiple Coordination of CO on Molybdenum Nanoparticles: Evidence for Intermediate $Mo_x(CO)_y$ Species by XPS and UPS

Zhiquan Jiang,[†] Weixin Huang,[‡] Zhen Zhang,[†] Hong Zhao,[†] Dali Tan,[†] and Xinhe Bao*,[†]

State Key Laboratory of Catalysis, Dalian Institute of Chemical Physics, Chinese Academy of Sciences, Dalian 116023, China, and Department of Chemical Physics, University of Science and Technology of China, Hefei 230026, China

Received: August 16, 2006; In Final Form: October 8, 2006

CO chemisorption on the metallic molybdenum nanoparticles supported on the thin alumina film was investigated by X-ray photoelectron spectroscopy (XPS) and ultraviolet photoelectron spectroscopy (UPS). A binary compound of molybdenum and CO is found to be formed on the surface upon CO dose, accompanied with a positive binding energy shift of the Mo 3d doublet and a localized Mo 4d valence band. A loose packing of the metallic molybdenum favors the formation of this intermediate $Mo_x(CO)_y$ species. The formation of the $Mo_x(CO)_y$ species implies that the property of the metallic molybdenum nanoparticles on the thin alumina film is much different from that of the bulk molybdenum, indicating a significant nanometer size effect.

Introduction

Industrial catalysts are often made of metal particles (1−10 nm) supported on ill-defined oxide powders. The adsorption behavior and reactivity of metal particles and deposits on oxide supports is still a highly relevant topic, especially with respect to the field of heterogeneous catalysis. Because of a high surface-to-volume ratio and the coexistence of different facets, these particles may show enhanced efficiencies and selectivities for chemical reactions compared to plane surfaces.[1] One of the aims of heterogeneous catalytic research is the understanding of the observed size-dependent catalytic behavior of supported metal particles on a molecular level.[2] The oxygen-storage mechanism and its size dependence were observed on the supported Pd nanoparticles, and this particle-size-dependent oxidation and reduction phenomena would likely have to be considered in the development of realistic microkinetic descriptions of catalytic reactions.[3] One approach came from ultrahigh-vacuum (UHV) surface science studies, using different crystal planes to model the active sites of real catalysts.[4] Other model catalysts, consisting of metal particles supported on oxide surfaces, were introduced to bridge shortcomings introduced by single-crystal studies.[5] Particles of nanometer size (nanoparticles) supported on well-characterized oxide surfaces are of particular interest to model the high complexity of real catalysts to answer questions such as the role of intrinsic size effects and the influence of the support.[6] The oxide films (Al_2O_3, SiO_2, TiO_2, MgO) used are thin enough to be suitably conductive for use with various electron-based spectroscopies.[7] On the other hand, these supported model catalysts can also simulate the critical features of most practical high surface area metal catalysts. In these studies, the metal particles were so small that size effects became important and remarkable changes in chemical reactivities were observed. The nanometer size effect (or electronic structure) plays a major role for catalytic activities. Statistical probe methods such as thermal desorption spectroscopy (TDS), Fourier transform infrared (FTIR) spectroscopy, X-ray photoelectron spectroscopy (XPS), and ultraviolet photoelectron spectroscopy (UPS) were employed for the study of adsorption and reactions on nanoparticles. Many surface scientists have been carrying out extensive experimental as well as theoretical studies to unveil the origin of the unusually high catalytic activities of nanoparticles with respect to the bulk counterparts. The metal−oxygen interaction changed as a function of the particle size at the nanoscale, which could cause an interesting size selectivity in a heterogeneously catalyzed reaction.[8] The change of the cluster size affects the adsorption property of the adsorbates on the metallic nanoparticles via modification of the electronic structure, thereby influencing the reactivities and reaction paths. A size-dependent transition of the chemical nature of chemisorption on small atomic clusters was reported by Burkart et al.[9]

It has been experimentally found and theoretically predicted that CO is prone to dissociative adsorption on several early transition metals. The thermally induced dissociation of CO was observed on a Mo(110) surface by means of high-resolution core-level spectroscopy.[10] At low coverage CO, dissociation could start at temperatures as low as 125 K whereas at saturation CO coverage, no dissociation occurred below 280 K. The reasons for this difference in dissociation behavior were concluded to be steric effects. The dissociative adsorption of CO on the bulk molybdenum was also observed on other single-crystal planes.[11,12] Because of a strong electron back-donation to the $2\pi^*$ antibonding orbital of the adsorbed CO, the CO molecules are tilted away from the surface normal. Tilting allows for a greater overlap of the CO $2\pi^*$ antibonding orbitals with the valence levels of the metal substrate. This increased overlap may facilitate charge donation from metal states into the antibonding $2\pi^*$ orbital thereby reducing the strength of the C−O bond, and hence the adsorbed CO on the bulk molybdenum exhibits significantly low vibrational frequencies below 1500 cm^{-1}.[13,14] This species was proposed to be a precursor state for CO dissociation. Additionally, associative recombina-

* To whom correspondence should be addressed. Tel.: +86-411-84686637; fax: +86-411-84694447; e-mail: xhbao@dicp.ac.cn.
[†] Dalian Institute of Chemical Physics.
[‡] University of Science and Technology of China.

10.1021/jp065293i CCC: $33.50
Published on Web 11/23/2006

tion of the dissociated CO on Mo(100) is observed at 900, 1024, and 1240 K.[15] However, a desorption signal for 28 amu was observed at ~240 K on the metallic molybdenum nanoparticles supported on the thin alumina film, even with a very small dose of CO at liquid nitrogen temperature.[16] This was attributed to the molybdenum carbonyl-like species formed by the multiple coordination of CO on the molybdenum nanoparticles. In this study, more evidence for the formation of this intermediate carbonyl-like species were acquired by XPS and UPS on the metallic molybdenum nanoparticles deposited on the thin Al_2O_3 film.

Experimental

Experiments of photoelectron spectroscopy were performed on an Omicron multiprobe surface analysis system with a base pressure of below 2.0×10^{-10} mbar, as described in detail elsewhere.[17] In brief, the system was equipped with facilities for XPS and UPS. XPS data were collected by Mg Kα radiation ($h\nu = 1253.6$ eV) with a power of 300 W. All UP spectra were recorded at detection angles perpendicular to the sample surface with He I radiation ($h\nu = 21.2$ eV), and the photoelectron peak positions were calibrated with respect to the Fermi level of the clean Re(0001) substrate. A Re(0001) single crystal was mounted on an Omicron sample holder and was resistively heated by a PBN (pyrolytic boron nitride) heater. The sample temperature was monitored by a chromel−alumel thermocouple spot-welded on the back side of the metallic substrate. The sample was cleaned by standard procedures, including oxidation, Ar^+ ion sputtering, and annealing at a high temperature until no contaminants could be detected by XPS. A homemade aluminum evaporator was used to prepare the thin Al_2O_3 film. Molybdenum deposition on the alumina film was achieved via an electron-beam-assisted evaporator (Focus EFM3), which had been initially thoroughly degassed. The pressure was kept below 5.0×10^{-10} mbar during molybdenum deposition at room temperature. In all photoelectron spectroscopy measurements, 15 L exposure of CO was introduced onto the sample surface by backfilling the chamber.

Results and Discussion

It was previously reported that a thin alumina film was prepared as a catalyst support by deposition and oxidation of aluminum on a Pt(110) substrate in a UHV system, and then molybdenum was deposited on this oxide film via thermal decomposition of $Mo(CO)_6$. After heated to 1200 K, surface molybdenum stayed on the surface in its metallic form, which was designated as the Mo/Al_2O_3 model catalyst.[18] CO desorption from this model catalyst exhibits a wide and intense feature ranging from 400 to 600 K, which corresponds to CO desorption from the Al_2O_3 film. Maybe the thin oxide film is not so perfect at the atomic level that many coordinatively unsaturated Al^{3+} sites are exposed on the oxide surface because of the surface defect. These Al^{3+} sites provide an opportunity for the strongly adsorbed CO molecules on the thin Al_2O_3 film. Specifically, a weak but distinct peak appears at approximately 240 K at small exposures of CO and gains in intensity with increasing CO exposure.[16] The 240 K signal was not observed on the thin alumina film or on the MoO_3/Al_2O_3 model surface. This low-temperature feature is therefore relevant to the metallic molybdenum nanoparticles on the Al_2O_3 film. Additionally, this signal is very close to molecular desorption of $Mo(CO)_6$ from the Mo/Al_2O_3 model catalyst in desorption temperature at maximum intensity; thus, it likely corresponds to molecular desorption of an intermediate molybdenum carbonyl-like species formed on the surface, which is denoted as $Mo_x(CO)_y$. Approach to saturation of the ~240 K peak at large CO exposure also confirms that this desorption signal is trustworthily correlated with the metallic molybdenum nanoparticles on the surface. It indicates that when CO is exposed to the Mo/Al_2O_3 model catalyst at liquid nitrogen temperature, CO coordinates strongly the metal nanoparticles and forms the intermediate $Mo_x(CO)_y$ species, which is stable up to ~240 K and then is desorbed molecularly at elevated temperatures.

To acquire more evidence for the formation of this intermediate $Mo_x(CO)_y$ species, XPS and UPS techniques in the Omicron UHV system were employed for CO chemisorption on the metallic molybdenum nanoparticles at liquid nitrogen temperature. A thin and homogeneous alumina film, prepared by deposition and oxidation of aluminum on a refractory Re(0001) substrate, was annealed at 1200 K under UHV conditions. High-resolution electron energy loss spectroscopy (HREELS) demonstrates that the oxide film is long-range ordered and free from surface hydroxyl groups, and XPS and UPS results indicate that the film is essentially stoichiometric.[17] Then, molybdenum was deposited by physical vapor deposition on this oxide film at room temperature. The temperature-dependent changes of the Mo 3d, Al 2s, and O 1s XPS of the Mo/Al_2O_3/Re(0001) system (not shown) indicate that a strong interaction occurs between the metallic molybdenum and the Al_2O_3 substrate. In the viewpoint of thermodynamics (the data of the pure compounds from),[19] the surface molybdenum species still maintains its metallic nature when the Mo/Al_2O_3 sample is heated up to 1000 K.

UPS was applied to monitor the valence band change of the Mo/Al_2O_3 model surface upon annealing, as shown in Figure 1. The photoelectron peak positions were calibrated with respect to the Fermi level of the clean Re(0001) substrate (Figure 1a). The UPS on the thin Al_2O_3 film exhibits an intense feature at 6.9 eV and two shoulder peaks at 9.3 and 11.4 eV below the Fermi level. The features in the binding energy range 5−12 eV are the valence bands of Al_2O_3, comprising mainly Al 3s and O 2p states.[17,20] The valence band emission of the Al_2O_3 substrate reduces its intensity after molybdenum deposition at room temperature because of the hindrance of the photoemission by the deposited metallic molybdenum. Additionally, a new signal develops at 1.70 eV below the Fermi level, corresponding to the photoemission of Mo 4d valence band on the surface. When the sample was heated, the O 2p-derived valence band feature slightly gains in intensity, indicating that a part of the Al_2O_3 substrate is exposed again because of the occurrence of molybdenum agglomeration upon annealing. Simultaneously, the photoemission of the Mo 4d valence band moves toward lower binding energy. This change of the Mo 4d feature is also attributed to the increased molybdenum particle size induced by thermal annealing. When Cu was deposited onto α-Al_2O_3-(0001), the emission feature of the Cu 3d valence band was observed to move toward lower binding energy with increasing Cu coverage.[21] Valence-band narrowing and a shifting of the core lines toward higher binding energies with decreasing cluster size were generally observed.[20] The former was considered to be an initial-state effect and was commonly used to characterize the nonmetal-to-metal transition of the clusters, whereas the latter was assigned in most cases to a final-state effect dominated by the coulomb interaction induced by the charge left on the clusters following the emission of photoelectrons.[22] The dynamical final-state effect was believed to lead to a systematic asymmetric broadening of all spectral features.[23] Additionally, the final-state coulomb charge does not only lead to a shift of the core levels but also to a shift of the valence levels and Fermi

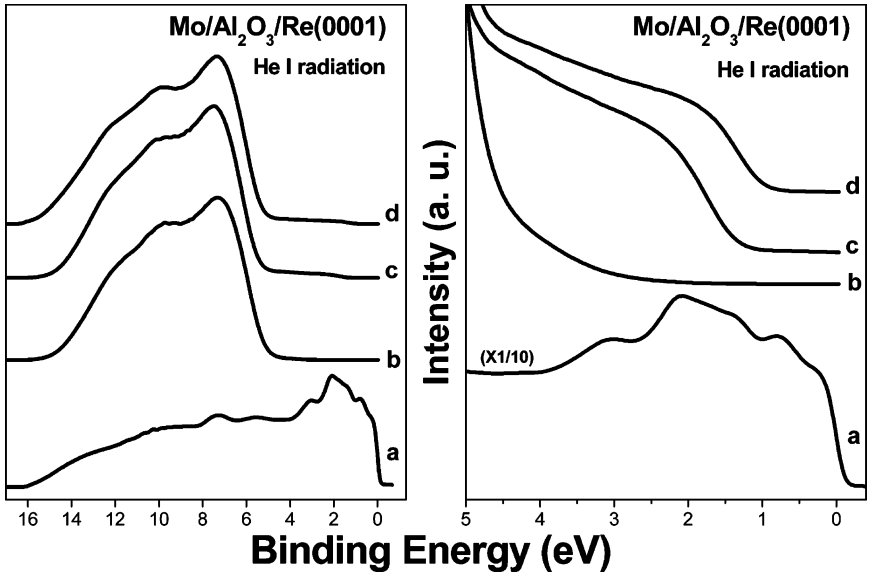

Figure 1. A series of UPS of (a) a clean Re(0001) surface, (b) a clean Al_2O_3 film, and (c) molybdenum deposition on the Al_2O_3 film at 300 K and then (d) annealed at 1000 K.

edge as well, since the charge is the same, no matter where the electron originates from. However, the Mo 4d valence band edge locates at 1.36 eV upon 1000 K annealing, far below the Fermi level of the bulk molybdenum, which is identical to that of the Re substrate. One should take into account that the shift of the valence band can be caused by the final state effect, as Hövel and many other scientists have been showing.[24] However, the oxide substrate is thin enough to decrease or even eliminate the surface-charge problem during the photoemission process. The final state effect is therefore not considered to be the primary source for the large valence band shift of the molybdenum nanoparticles. Moreover, although the charge transfer from metallic molybdenum to the Al_2O_3 substrate takes place, as illustrated by the XPS measurements, it has a little contribution to this large shift of the onset of the Mo 4d valence band. Therefore, the valence band shift of the metallic molybdenum nanoparticles on the thin Al_2O_3 film is mainly the consequence of nanometer size effect on the metallic clusters. Because of their finite small sizes, these small particles have a discrete electron density of states (DOS) and thereby totally different structures and "materials properties" from their bulk crystalline counterparts. Considering that charge transfer from metal to adsorbate is generally crucial for the dissociative adsorption, the nondissociative adsorption on nanoparticles may be related to lower electron densities in nanoparticles with respect to the bulk counterparts. This electronic structure of the molybdenum nanoparticles extremely weakens the electron back-donation from the d orbitals of the metallic particles to the π^* orbitals of the adsorbed CO molecules. The weakness of the electron back-donation likely causes CO to adsorb molecularly on the metallic molybdenum nanoparticles, not as in the case on the bulk molybdenum, where CO undergoes dissociation because of the strong d$-\pi$ electron back-donation.[12] The molecular adsorption of CO on the metallic molybdenum nanoparticles is probably responsible for the formation of the intermediate $Mo_x(CO)_y$ species, which was observed to desorb from the surface at 240 K in the TDS.

CO chemisorption on the metallic molybdenum nanoparticles was investigated by means of XPS and UPS to find some evidence for the formation of the intermediate $Mo_x(CO)_y$ species. Figure 2 shows a series of Mo 3d XPS of the Mo/Al_2O_3 model surface upon CO dose and subsequent annealing at the indicated

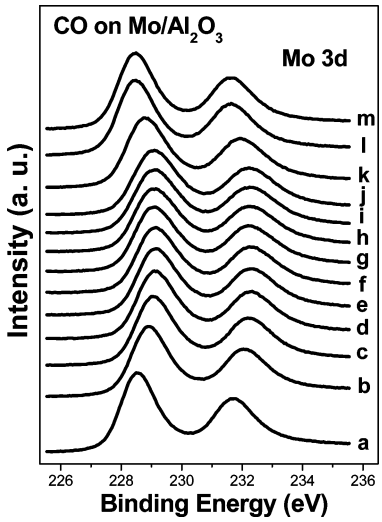

Figure 2. Mo 3d XPS of CO adsorbed on the Mo/Al_2O_3 model surface. (a) A clean Mo/Al_2O_3 model surface; after CO dose on the Mo/Al_2O_3 surface at 100 K, the sample was annealed at (b) 100 K, (c) 150 K, (d) 200 K, (e) 250 K, (f) 300 K, (g) 400 K, (h) 500 K, (i) 600 K, (j) 700 K, (k) 800 K, (l) 900 K, and (m) 1000 K.

temperatures. The Mo $3d_{5/2}$ peak locates at 228.5 eV on the clean Mo/Al_2O_3 model surface, while it moves to 228.9 eV upon CO chemisorption at 100 K. The positive binding energy shift of the Mo 3d doublet suggests that CO molecularly adsorbs on the metallic molybdenum nanoparticles. The electron back-donation from the metallic molybdenum to the adsorbed CO causes the Mo 3d doublet to shift toward higher binding energy. Slightly increasing the sample temperature, the Mo $3d_{5/2}$ peak further moves upward, with binding energy of 229.1 eV at 200 K. This is explained by the bonding between the adsorbed CO and the molybdenum nanoparticles strengthening at elevated temperatures, causing more electrons to transfer from the underlying molybdenum to the CO. Hereafter, the Mo 3d doublet remains the same over a relatively wide temperature range, till the sample is heated up to 600 K. However, the multiple coordination configuration of CO is stable up to ~240 K on the Mo/Al_2O_3 model surface, and the intermediate $Mo_x(CO)_y$ species is observed to desorb at 240 K in the TDS. The dissociation of partial CO admolecules occurs in the presence

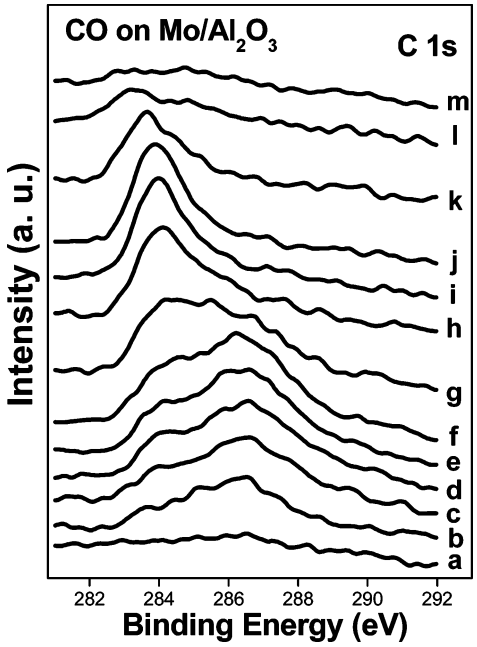

Figure 3. C 1s XPS of CO adsorbed on the Mo/Al_2O_3 model surface. (a) A clean Mo/Al_2O_3 model surface; after CO dose on the Mo/Al_2O_3 surface at 100 K, the sample was annealed at (b) 100 K, (c) 150 K, (d) 200 K, (e) 250 K, (f) 300 K, (g) 400 K, (h) 500 K, (i) 600 K, (j) 700 K, (k) 800 K, (l) 900 K, and (m) 1000 K.

of the metallic molybdenum nanoparticles upon annealing, and some oxygen species is left on the molybdenum, resulting in constant binding energy of the Mo 3d doublet over a wide temperature range between 200 and 600 K. Then, the Mo $3d_{5/2}$ peak moves toward lower binding energy with continually increasing the sample temperature, and upon 1000 K annealing restores the peak position to the clean surface condition. The adsorbed CO undergoes desorption from the surface or dissociation by the underlying metallic molybdenum at elevated temperatures.

C 1s XPS of CO chemisorption on the Mo/Al_2O_3 model surface also illustrates that CO initially adsorbs in the molecular form, as shown in Figure 3. When CO was exposed to the Mo/Al_2O_3 model surface at 100 K, a signal appears at 286.4 eV for the molecularly adsorbed CO. This C 1s XPS feature is very broad, indicating that CO molecules adsorb in various coordination forms. Coordinative unsaturation occurs on the edge or corner atoms of the metallic nanoparticles, which provides an opportunity for the CO to adsorb in multiple coordination form. With increasing the sample temperature, a new emission signal appears at 284.1 eV and gradually gains its intensity with the expense of the molecularly adsorbed CO signal at 286.4 eV. It implies that multiple coordination of the molecularly adsorbed CO on the Mo/Al_2O_3 surface is destroyed and decomposed upon annealing. The new signal dominates the C 1s feature when heated up to 400 K. This peak moves toward lower binding energy with further increasing the sample temperature and continues to gain its intensity, approaching its maximum upon 700 K annealing. A part of the molecularly adsorbed CO desorbs from the surface, while the rest undergoes dissociation in the presence of the metallic molybdenum particles to leave some carbon on the model surface. Under the effect of high temperature, the carbon species and the metallic molybdenum interact strongly, and the molybdenum carbide species forms on the surface, inducing negative binding energy shift of the C 1s feature. When the sample was annealed at 1000 K, no distinct C 1s feature is detected on the surface, indicating that the formed molybdenum carbide species has been reduced by the oxygen contained in the thin Al_2O_3 film.

Figure 4 illustrates comparison of the C 1s and Mo 3d regions for various model systems: the clean Mo/Al_2O_3 model surface, CO exposure on the thin Al_2O_3 film and the Mo/Al_2O_3 model surface, and $Mo(CO)_6$ exposure on the thin Al_2O_3 film. When CO was dosed on the thin Al_2O_3 film, a weak signal appears at 286.9 eV for the adsorbed CO molecules. A broad peak appears at 286.4 eV upon CO dose on the Mo/Al_2O_3 model surface, lower in binding energy than that on the thin Al_2O_3 film. This can be explained by the model of electron transfer and back-donation. CO adsorbs on coordinatively unsaturated Al^{3+} site via a σ bond; however, no electron back-donation occurs from the thin Al_2O_3 film to the adsorbed CO, since there are no d electrons contained in the Al^{3+} ions. This charge transfer between the adsorbed CO and the Al_2O_3 substrate causes C 1s to locate at a higher binding energy. On the Mo/Al_2O_3 model surface, a distinct signal appears at 286.4 eV for the molecularly adsorbed CO, since the peak corresponding to the dissociated CO should lie at 284.5 eV. The intensity of the C 1s peak on the Mo/Al_2O_3 model surface is much larger than that on the thin Al_2O_3 film. Nevertheless, the binding energy of this signal does not reach the value of 287.8 eV upon $Mo(CO)_6$ chemisorption on the thin Al_2O_3 film, only similar to that of molybdenum subcarbonyls, which were formed by partial thermal decomposition of $Mo(CO)_6$ with increasing the sample temperature.[17] Compared to the clean Mo/Al_2O_3 model surface, CO chemisorption causes the Mo 3d doublet to move toward higher binding energy, because the electron back-donation occurs from the metallic molybdenum nanoparticles to the adsorbed CO. However, the Mo 3d doublet does not reach the value of 229.2 eV upon $Mo(CO)_6$ chemisorption on the thin Al_2O_3 film, also in excellent agreement with that of the surface molybdenum subcarbonyls species.[17] Both C 1s and Mo 3d signals upon CO exposure to the Mo/Al_2O_3 model surface are well consistent in binding energy with those of the molybdenum subcarbonyls, indicating that an intermediate molybdenum subcarbonyl-like species is formed upon CO dose at 100 K. Therefore, the multiple coordination of the molecularly adsorbed CO is formed on the metallic molybdenum nanoparticles.

CO chemisorption on the metallic molybdenum nanoparticles was also investigated by UPS, illustrated in Figure 5 as a function of the substrate temperature. The difference spectra shown in the bottom panel were obtained by subtracting the spectrum on the surface annealed at the indicated temperatures from the initial spectrum (a) of the Mo/Al_2O_3 model surface. When CO was dosed to the Mo/Al_2O_3 model surface at 100 K, distinct features were observed at 12.0 and 9.0 eV, corresponding to the valence band emission of the 4σ and $1\pi + 5\sigma$ orbitals in the adsorbed CO molecules, respectively. The negative peaks at 10.1 and 7.5 eV in the difference spectrum are derived from the inhibition and suppression of the valence band emission on the thin Al_2O_3 film by the adsorption layer of CO. With increasing the sample temperature, the valence band emission for the adsorbed CO reduces the intensity and slightly moves toward higher binding energy. Simultaneously, the negative peaks in the bottom panel decrease the intensity, illustrating that the thickness of the adsorption layer decreases and hence the suppression of the photoemission of the oxide substrate weakens. It implies that the adsorbed CO molecules undergo desorption or decomposition upon annealing. For Mo 4d valence band emission, we focus on the change of CO chemisorption on the Mo/Al_2O_3 model surface in the binding energy region between 0 and 5 eV, as shown in the right panel of Figure 5.

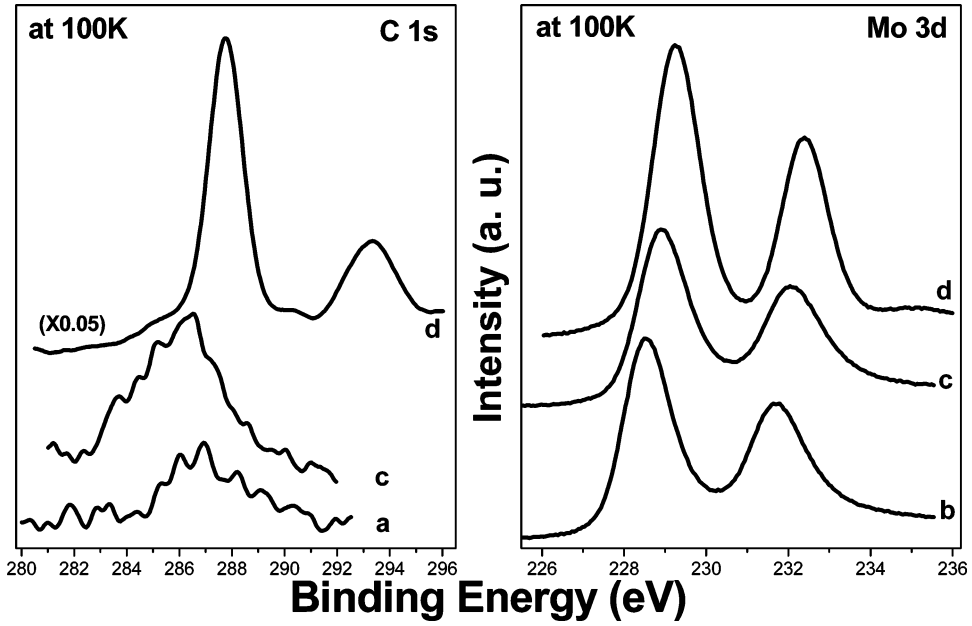

Figure 4. Comparison of C 1s and Mo 3d regions for (a) CO exposure on Al_2O_3 film, (b) clean Mo/Al_2O_3 surface, (c) CO exposure on Mo/Al_2O_3 surface, and (d) $Mo(CO)_6$ exposure on Al_2O_3 film.

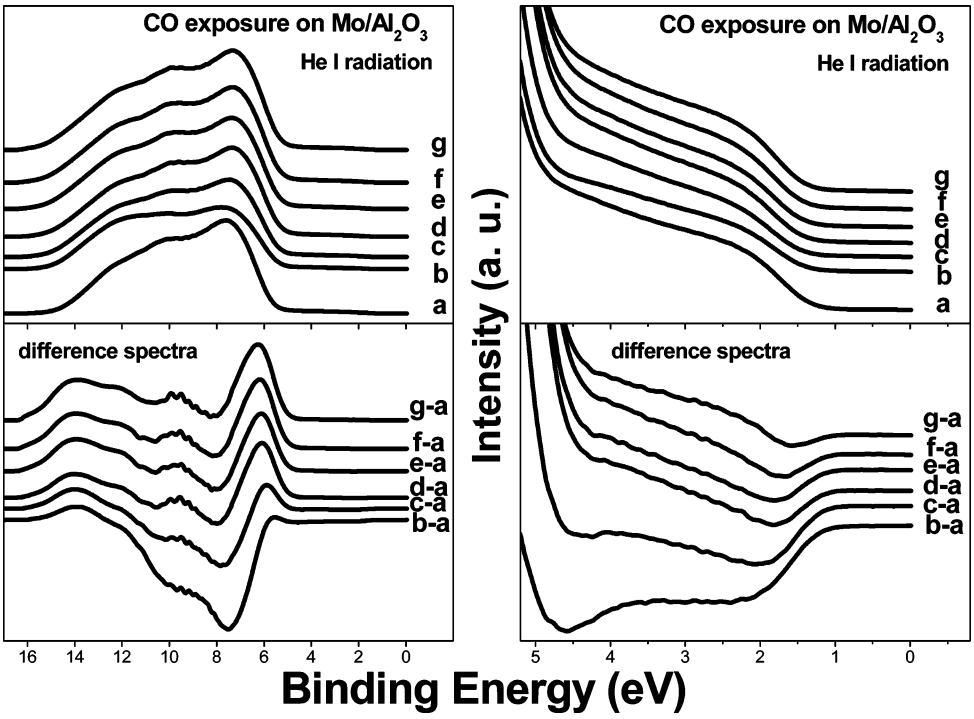

Figure 5. UPS of CO adsorbed on the Mo/Al_2O_3 model surface. (a) A clean Mo/Al_2O_3 model surface; after CO dose on the Mo/Al_2O_3 surface at 100 K, the sample was annealed at (b) 100 K, (c) 150 K, (d) 250 K, (e) 300 K, (f) 400 K, and (g) 500 K. The difference spectra shown in the bottom panel were obtained by subtracting the spectrum on the surface annealed at the indicated temperatures from the initial spectrum (a) of the Mo/Al_2O_3 model surface.

When CO was dosed to the Mo/Al_2O_3 model surface at 100 K, the Mo 4d valence band emission moves toward higher binding energy and drastically decreases its intensity. It is interesting that a positive emission appears at 3.5 eV in the difference spectrum upon CO chemisorption. This implies that the valence electrons in the Mo 4d band are partially localized, resulting in the positive signal similar to that of molybdenum subcarbonyls. With increasing the sample temperature, the Mo 4d valence band emission moves toward lower binding energy and gradually gains its intensity; at the same time, the positive peak at 3.5 eV reduces its intensity and eventually disappears upon 400 annealing. This also suggests that desorption or decomposition of the adsorbed CO molecules occurs when heating the sample. The multiple coordination of the molecularly adsorbed CO collapses at elevated temperature, in accordance with the TDS results.

Figure 6 displays comparison of difference UPS for several model systems: CO exposure on the thin Al_2O_3 film and the Mo/Al_2O_3 model surface and $Mo(CO)_6$ exposure on the thin Al_2O_3 film. The difference spectrum was obtained by subtracting the spectrum on the surface after expose to the adsorbates from the initial spectrum of the corresponding clean surface. When CO was exposed to the Mo/Al_2O_3 model surface at 100 K, the valence band emission is observed at 8.8 eV in binding energy

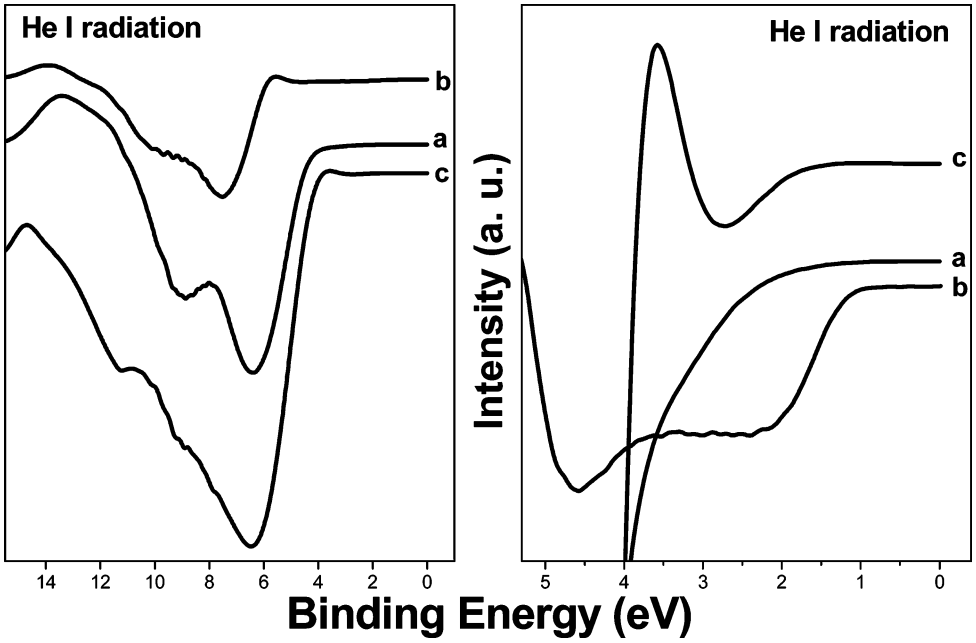

Figure 6. Comparison of difference UPS for (a) CO exposure on the thin Al_2O_3 film, (b) CO exposure on the Mo/Al_2O_3 model surface, and (c) $Mo(CO)_6$ exposure on the thin Al_2O_3 film. The difference spectrum was obtained by subtracting the spectrum on the surface after expose to the adsorbates from the initial spectrum of the corresponding clean surface.

for the $1\pi + 5\sigma$ orbitals in the adsorbed CO, higher than that in the case of CO exposure on the thin Al_2O_3 film but still lower than that in the case of $Mo(CO)_6$ exposure on the thin Al_2O_3 film. The binding energy of this valence band emission is well consistent with that of molybdenum subcarbonyls, indicating that an intermediate carbonyl-like species is formed on the Mo/Al_2O_3 model surface upon CO chemisorption. The formation of this intermediate carbonyl-like species is also evidenced by the difference spectra of the Mo 4d valence band, as shown in the right panel of Figure 6. When CO was dosed to the Mo/Al_2O_3 model surface, a weak but distinct emission appears at 3.5 eV for the Mo 4d valence band, which is absent in the case of CO exposure on the thin Al_2O_3 film. Although this emission is much weaker in intensity than that in the case of $Mo(CO)_6$ exposure on the thin Al_2O_3 film, the binding energy of the Mo 4d valence band agrees well with that of $Mo(CO)_6$ on the thin Al_2O_3 film. This phenomenon further confirms that the intermediate carbonyl-like species is formed on the Mo/Al_2O_3 model surface upon CO exposure at 100 K. That is to say, a highly coordinated surface species is formed on the metallic molybdenum nanoparticles by molecular adsorption of CO, which causes the electron density of states (DOS) of the metal particles to grow discrete. The appearance of this multiple coordination of the molecularly adsorbed CO suggests that the property of the metallic molybdenum nanoparticles on the thin Al_2O_3 film is totally different from that of the bulk molybdenum.

There are many gas-phase studies showing different chemisorption properties of gas molecules on small metal clusters with respect to the respective bulks. Molecular chemisorption was often found to be preferred to the dissociative chemisorption on small metal clusters, while it can efficiently dissociate diatomic molecules in the bulk form.[25] CO was exposed to the mass-selected negatively charged Ni_n^- and Pt_n^- clusters, and the $Ni_n(CO)_m^-$ and $Pt_n(CO)_m^-$ clusters were formed; saturation with CO in clusters could be detected, which was caused by the formation of an electronic closed shell and which was not caused by steric hindrance between neighboring COs as on a surface.[26] The multiple coordination configuration of the molecularly adsorbed CO on the oxide-supported clusters was previously observed on other systems. The $[Ru_6C]$ clusters on the MgO carriers were observed to be transformed into the $[Ru_6C(CO)_{11}]$ clusters by means of DXAFS (energy-dispersive X-ray absorption fine structure) technique when exposed to CO/H_2 reaction gases.[27] The formation of Rh dicarbonyl species on the γ-Al_2O_3 surface, as monitored by XANES (X-ray absorption near-edge spectroscopy) and time-resolved DXAFS,[28] is in accordance with the previous IR results.[29] The effect of CO on the morphology of Pt nanoparticles was also detected on $TiO_2(110)-(1 \times n)$ by means of STM, which was explained by CO-assisted Ostwald ripening, in which the mass transport proceeded via surface carbonyl intermediates.[30] The formation of the intermediate transition-metal carbonyl was also observed on rhodium[31] and palladium[32−35] particles deposited on a well-ordered alumina substrate by means of TDS, XPS, UPS, and IR spectra. However, the TDS intensity of the intermediate $Mo_x(CO)_y$ species formed on the thin alumina film is much less remarkable compared to that of the $Pd_x(CO)_y$ species in refs 32 and 33. This may be due to the difference in the formation condition of the metal carbonyls. The Mo/Al_2O_3 model catalyst was formed by annealing up to 1200 K after molybdenum deposition on the thin alumina film, which led to a serious sintering of the surface molybdenum nanoparticles, deduced by a decrease of the Mo 3d XPS intensity as a function of sample temperature.[18] The sintering drastically reduces the cross section of interaction between the adsorbed CO and the surface molybdenum nanoparticles, consequently decreasing the amount of the intermediate $Mo_x(CO)_y$ species. If the sintering was reduced, desorption of the $Mo_x(CO)_y$ species would grow intense.

According to the above speculation, the metallic molybdenum model catalyst was prepared on the thin alumina film with a reduced sintering. CO chemisorption and desorption were performed on this model catalyst, and only one desorption signal was observed at ~260 K with exposure to 15.0 L CO.[16] No CO desorption was contributed from the alumina film, indicating that the deposited molybdenum covers nearly all the surface of the thin alumina film. Mo metal dissociated CO effectively; only for high exposures, where dissociated CO was saturated, was

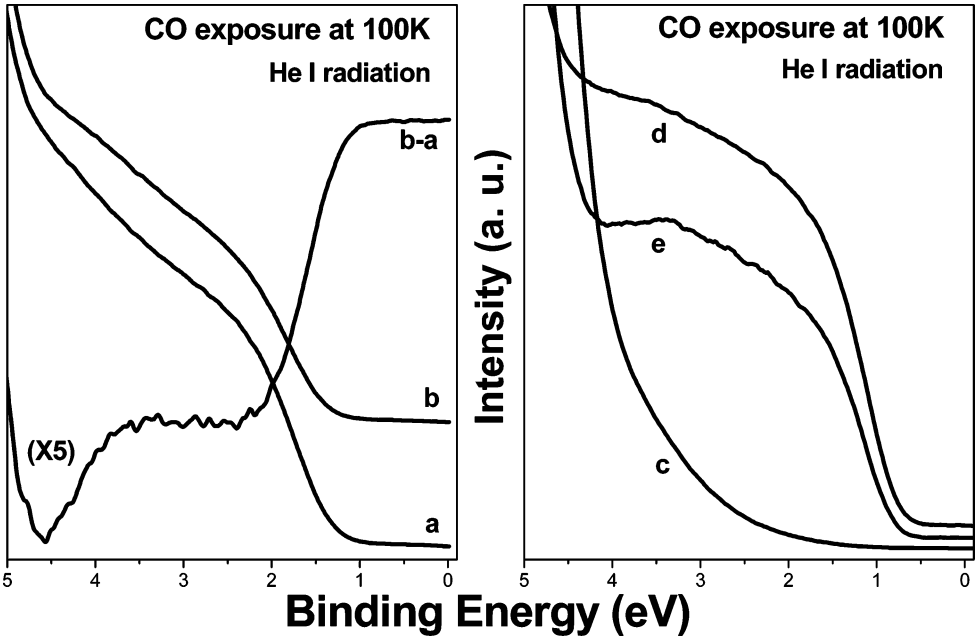

Figure 7. UPS of several model systems: (a) Mo(1000 K)/Al_2O_3 surface, (b) CO exposure on Mo(1000 K)/Al_2O_3 surface, (c) thin Al_2O_3 film, (d) Mo(300 K)/Al_2O_3 surface, and (e) CO exposure on Mo(300 K)/Al_2O_3 surface.

molecularly adsorbed CO observed at about 310 K.[36] Therefore, the desorption signal is due to the intermediate molybdenum carbonyl-like species formed on the surface upon CO dose. This desorption intensity is much larger than that on the molybdenum model catalyst annealed at 1200 K, indicating that a loose packing of the deposited molybdenum is favorable for the formation of the intermediate $Mo_x(CO)_y$ species. The molybdenum particle annealed at 700 K is much smaller than that annealed at 1200 K, which allows for a higher degree of Mo−CO coordination at liquid-nitrogen temperature. This nanometer size effect was also observed on the palladium clusters grown onto the alumina substrate at different temperatures, as evidenced by UPS and XPS.[33,34]

UPS results also illustrate that the loose packing of the metallic molybdenum favors the formation of this intermediate $Mo_x(CO)y$ species upon CO dose. When CO was dosed to the Mo/Al_2O_3 model surface annealed at 1000 K, no distinct feature is observable in the UP spectrum and only a weak feature is present at 3.5 eV in the difference spectrum, as shown in the left panel of Figure 7. However, on the Mo/Al_2O_3 model surface which was not annealed at elevated temperatures after molybdenum deposition at room temperature, a distinguished feature appears at 3.4 eV in the UP spectrum (curve e). It implies that more of the Mo 4d valence electrons are localized on the unannealed Mo/Al_2O_3 model surface, indicating the formation of more intermediate carbonyl-like species upon CO chemisorption than on the Mo/Al_2O_3 model surface annealed at 1000 K.

The valence band edge of the metallic molybdenum nanoparticles on the thin Al_2O_3 film is much lower than the Fermi level of the bulk molybdenum, which should reduce the ability of electron back-donation from the metal nanoparticles to the $2\pi^*$ orbitals of the adsorbed CO. The reduction of the so-called π back-donation would result in weaker metal−CO bonds and would make difficult the dissociation of CO.[37] Consequently, it is possible for CO to form molecular adsorption on the molybdenum nanoparticles instead of dissociative adsorption on the bulk molybdenum. The weak adsorption of CO was also observed on the molybdenum nanoclusters, which were deposited onto a Au(111) surface by thermal decomposition of $Mo(CO)_6$.[38] Mo nanoclusters bonded to the Au(111) surface exhibited a surprisingly low reactivity toward CO. Mo/Au(111) surfaces with Mo coverages below 0.1 ML adsorbed the CO molecule weakly (desorption temperature < 400 K) and did not induce C−O bond cleavage. For comparison, temperatures around 600 K are needed to desorb CO from Mo(110) at low coverages.[14] As the Mo coverage increased, the Mo−Mo interactions became more important than the Mo−Au interactions. In this respect, the "length scale" of the system is important, and special chemical properties are only observed for small Mo nanoparticles. On the Mo/Au(111) interface, the presence of CO prevented Mo−Au intermixing and, thus, enhanced the mobility of Mo on the surface. Large coverages of CO favored the permanence of Mo on the surface, opening the possibility for the formation and migration of $Mo_x(CO)_y$ aggregates. These aggregates would move around on the surface until finding special nucleation sites where the loss of CO took place and the Mo core partially sank into the Au substrate.[39] Adsorbed CO may reduce both Mo−Mo and Mo−Au interactions with the net result of Mo clusters weakly bonded to the Au surface. Indeed, there was precedence for enhanced mobility of Pt induced by adsorbed CO.[40] According to the density functional calculations, the CO molecules should be able to bring Mo atoms from the bulk of gold to above the surface giving them extra mobility.[41] Reversibility in the formation of stoichiometric surface molybdenum carbonyl was also observed on γ-alumina.[42] Later, infrared spectroscopic characterization found the formation of molybdenum carbonyl species by ultraviolet photoreduction of silica-supported Mo(VI) in carbon monoxide.[43] In another case of laser-induced photochemical deposition from the group VIB hexacarbonyls, the addition of CO at relatively low pressures dramatically decreases the rate of decomposition from those hexacarbonyls, which was due to regeneration of hexacarbonyls by reaction between the photoproducts and the ambient CO.[44]

Coordinatively unsaturated molybdenum atoms are present on the nanoparticle surface, especially the atoms at the edges and corners. This highly coordinative unsaturation provides an opportunity for CO to form a molecularly adsorbed configuration with a multiple coordination. That is to say, an intermediate

carbonyl-like species, in which two or more COs bond to one molybdenum atom, is formed on the Mo/Al_2O_3 model surface upon CO dose. The formation of this intermediate $Mo_x(CO)_y$ species suggests that the property of the metallic molybdenum nanoparticles is much different from that of the bulk molybdenum, indicating a prominent nanometer size effect. When the sample was heated, the adsorbed CO should desorb from the surface. Therefore, the cleavage of the Mo−CO bonds is competitive with that of the Mo−Mo bonds. It is prone to rupture the Mo−Mo bonds in the multiple coordination of CO, specifically at the edges and corners of the metallic molybdenum nanoparticles. Then, the CO desorbs from the model surface with the coordinated molybdenum, resulting in the desorption signal at ~240 K in the TDS. On the Rh/Al_2O_3 catalyst, CO-induced disintegration process of surface rhodium clusters was investigated by means of time-resolved DXAFS:[28] The Rh−Rh bonds became weaker by further CO adsorption and the Rh cluster was completely disintegrated at 3000 ms, and rhodium dicarbonyl species were therefore formed on the Al_2O_3 surface. On $TiO_2(110)-(1 \times 2)$, a very rapid disintegration of the supported Rh nanoparticles of 1−2 nm to atomically dispersed Rh was observed at 300 K even after a few minutes exposure to a pressure of 10^{-1} mbar CO, whereas such a process was much slower for larger Rh particles.[45] In the case of the effect of CO, it was assumed that the formation of a strong adsorbate−Rh bond causes the cleavage of the weaker Rh−Rh bond.[46] The driving force behind this process was considered to be very likely the high bond energy of Rh−CO (185 kJ/mol) compared to that of the Rh−Rh bond (44.5 kJ/mol).[45−47] CO-induced morphology changes of Ir nanoparticles supported on TiO_2-$(110)-(1 \times 2)$ surface were likewise explained by the difference between the Ir−CO bond energy (159 kJ/mol) and the Ir−Ir bond energy (146 kJ/mol).[48] In other words, the formation of a strong Ir−CO bond results in rupture of the Ir−Ir bond.[49]

Conclusions

Molybdenum deposition onto the thin Al_2O_3 film was achieved by physical vapor deposition at room temperature. The valence band edge of the metallic molybdenum nanoparticles on the thin Al_2O_3 film is much lower than the Fermi level of the bulk molybdenum, as evidenced by UPS, which should reduce the ability of electron back-donation and make the molecular adsorption of CO possible. The TDS of CO on the Mo/Al_2O_3 model surface gives an extraordinary and distinct feature at ~240 K not present on the thin Al_2O_3 film and the MoO_3/Al_2O_3 model surface. XPS and UPS results also suggest that an intermediate molybdenum carbonyl-like species is formed on the Mo/Al_2O_3 model surface upon CO dose at 100 K. A loose packing of the metallic molybdenum is favorable for the formation of this intermediate $Mo_x(CO)_y$ species. The formation of this $Mo_x(CO)_y$ species is indicative of a prominent nanometer size effect on the metallic molybdenum nanoparticles, which are totally different from their bulk crystalline counterparts.

Acknowledgment. This work was financially supported by the National Natural Science Foundation of China (90206036).

References and Notes

(1) (a) Matolin, V.; Mâsek, K.; Elyakhloufi, M. H.; Gillet, E. *J. Catal.* **1993**, *143*, 492. (b) Goodman, D. W. *Chem. Rev.* **1995**, *95*, 523.

(2) (a) Che, M.; Bennett, C. O. *Adv. Catal.* **1989**, *36*, 55. (b) Nosova, L. V.; Stenin, M. V.; Nogin, Yu. N.; Ryndin, Yu. A. *Appl. Surf. Sci.* **1992**, *55*, 43.

(3) Schalow, T.; Brandt, B.; Starr, D. E.; Laurin, M.; Shaikhutdinov, S. K.; Schauermann, S.; Libuda, J.; Freund, H.-J. *Angew. Chem., Int. Ed.* **2006**, *45*, 3693.

(4) (a) Nakano, H.; Nakamura, I.; Fujitani, T.; Nakamura, J. *J. Phys. Chem. B* **2001**, *105*, 1355. (b) Nakao, K.; Ito, S.-I.; Tomishige, K.; Kunimori, K. *J. Phys. Chem. B* **2005**, *109*, 17553. (c) Nakao, K.; Ito, S.-I.; Tomishige, K.; Kunimori, K. *J. Phys. Chem. B* **2005**, *109*, 17579. (d) Nakao, K.; Ito, S.-I.; Tomishige, K.; Kunimori, K. *J. Phys. Chem. B* **2005**, *109*, 24002. (e) Haneda, M.; Nakamura, I.; Fujitani, T.; Hamada, H. *Catal. Surv. Asia* **2006**, *9*, 207.

(5) (a) Rainer, D. R.; Xu, C.; Goodman, D. W. *J. Mol. Catal. A* **1997**, *119*, 307. (b) Henry, C. R. *Surf. Sci. Rep.* **1998**, *31*, 231. (c) Stakheev, A. Yu.; Kustov, L. M. *Appl. Catal. A* **1999**, *188*, 3. (d) Bäumer, M.; Freund, H.-J. *Prog. Surf. Sci.* **1999**, *61*, 127.

(6) (a) Clair, T. P. St.; Goodman, D. W. *Top. Catal.* **2000**, *13*, 5. (b) Goodman, D. W. *J. Catal.* **2003**, *216*, 213. (c) Freund, H.-J. *Surf. Sci.* **2002**, *500*, 271. (d) Freund, H.-J.; Bäumer, M.; Libuda, J.; Risse, T.; Rupprechter, G.; Shaikhutdinov, S. *J. Catal.* **2003**, *216*, 223.

(7) Xu, C.; Oh, W. S.; Liu, G.; Kim, D. Y.; Goodman, D. W. *J. Vac. Sci. Technol., A* **1997**, *15*, 1261.

(8) Lim, D. C.; Lopez-Salido, I.; Dietsche, R.; Bubek, M.; Kim, Y. D. *Angew. Chem., Int. Ed.* **2006**, *45*, 2413.

(9) Burkart, S.; Blessing, N.; Ganteför, G. *Phys. Rev. B* **1999**, *60*, 15639.

(10) Jaworowski, A. J.; Smedh, M.; Borg, M.; Sandell, A.; Beutler, A.; Sorensen, S. L.; Lundgren, E.; Andersen, J. N. *Surf. Sci.* **2001**, *492*, 185.

(11) (a) Felter, T. E.; Estrup, P. J. *Surf. Sci.* **1976**, *54*, 179. (b) Guillot, C.; Riwan, R.; Lecante, J. *Surf. Sci.* **1976**, *59*, 581. (c) Ko, E. I.; Madix, R. J. *Surf. Sci.* **1980**, *100*, L505. (d) Semancik, S.; Estrup, P. J. *Surf. Sci.* **1981**, *104*, 26.

(12) Erickson, J. W.; Estrup, P. J. *Surf. Sci.* **1986**, *167*, 519.

(13) Zaera, F.; Kollin, E.; Gland, J. L. *Chem. Phys. Lett.* **1985**, *121*, 464.

(14) Chen, J. G.; Colaianni, M. L.; Weinberg, W. H.; Yates, J. T. *Chem. Phys. Lett.* **1991**, *177*, 113.

(15) Ko, E. I.; Madix, R. J. *Surf. Sci.* **1981**, *109*, 221.

(16) Jiang, Z. Q.; Zhao, H.; Tan, D. L.; Zhai, R. S.; Bao, X. H. *Chin. J. Catal.* **2005**, *26*, 423.

(17) Jiang, Z. Q.; Huang, W. X.; Zhang, Z.; Zhao, H.; Tan, D. L.; Bao, X. H. *Surf. Sci.*, in press.

(18) Jiang, Z. Q.; Huang, W. X.; Jiao, J.; Zhao, H.; Tan, D. L.; Zhai, R. S.; Bao, X. H. *Appl. Surf. Sci.* **2004**, *229*, 43.

(19) Lide, D. R. *CRC Handbook of Chemistry and Physics*, 86th ed.; CRC Press: Boca Raton, FL, 2005.

(20) Cai, Y. Q.; Bradshaw, A. M.; Guo, Q.; Goodman, D. W. *Surf. Sci.* **1998**, *399*, L357.

(21) Guo, Q.-L.; Møllert, P. J. *Vacuum* **1990**, *41*, 1114.

(22) (a) Mason, M. G. *Phys. Rev. B* **1983**, *27*, 748. (b) Kohiki, S.; Ikeda, S. *Phys. Rev. B* **1986**, *34*, 3786.

(23) Hövel, H.; Barke, I. *Prog. Surf. Sci.* **2006**, *81*, 53.

(24) (a) Hövel, H.; Grimm, B.; Pollmann, M.; Reihl, B. *Eur. Phys. J. D* **1999**, *9*, 595. (b) Hövel, H. *Appl. Phys. A* **2001**, *72*, 295. (c) Hövel, H.; Barke, I.; Boyen, H.-G.; Ziemann, P.; Garnier, M. G.; Oelhafen, P. *Phys. Rev. B* **2004**, *70*, 045424.

(25) (a) Kim, Y. D.; Stolcic, D.; Fischer, M.; Ganteför, G. *Chem. Phys. Lett.* **2003**, *380*, 359. (b) Kim, Y. D.; Ganteför, G. *Chem. Phys. Lett.* **2003**, *382*, 644.

(26) Icking-Konert, G. S.; Handschuh, H.; Ganteför, G.; Eberhardt, W. *Phys. Rev. Lett.* **1996**, *76*, 1047.

(27) Suzuki, A.; Yamaguchi, A.; Chihara, T.; Inada, Y.; Yuasa, M.; Abe, M.; Nomura, M.; Iwasawa, Y. *J. Phys. Chem. B* **2004**, *108*, 5609.

(28) Suzuki, A.; Inada, Y.; Yamaguchi, A.; Chihara, T.; Yuasa, M.; Nomura, M.; Iwasawa, Y. *Angew. Chem., Int. Ed.* **2003**, *42*, 4795.

(29) (a) Cavanagh, R. R.; Yates, J. T. *J. Chem. Phys.* **1981**, *74*, 4150. (b) Basu, P.; Panayotov, D.; Yates, J. T. *J. Am. Chem. Soc.* **1988**, *110*, 2074.

(30) Berkó, A.; Szökö, J.; Solymosi, F. *Surf. Sci.* **2004**, *566−568*, 337.

(31) (a) Bäumer, M.; Frank, M.; Libuda, J.; Stempel, S.; Freund, H.-J. *Surf. Sci.* **1997**, *391*, 204. (b) Frank, M.; Kühnemuth, R.; Bäumer, M.; Freund, H.-J. *Surf. Sci.* **1999**, *427−428*, 288. (c) Frank, M.; Kühnemuth, R.; Bäumer, M.; Freund, H.-J. *Surf. Sci.* **2000**, *454−456*, 968.

(32) Libuda, J.; Sandell, A.; Bäumer, M.; Freund, H.-J. *Chem. Phys. Lett.* **1995**, *240*, 429.

(33) Sandell, A.; Libuda, J.; Bäumer, M.; Freund, H.-J. *Surf. Sci.* **1996**, *346*, 108.

(34) Sandell, A.; Libuda, J.; Brühwiler, P. A.; Andersson, S.; Bäumer, M.; Maxwell, A. J.; Mårtensson, N.; Freund, H.-J. *Phys. Rev. B* **1997**, *55*, 7233.

(35) (a) Sandell, A.; Libuda, J.; Brühwiler, P.; Andersson, S.; Maxwell, A.; Bäumer, M.; Mårtensson, N.; Freund, H.-J. *J. Electron Spectrosc. Relat. Phenom.* **1995**, *76*, 301. (b) Wolter, K.; Seiferth, O.; Libuda, J.; Kuhlenbeck, H.; Bäumer, M.; Freund, H.-J. *Chem. Phys. Lett.* **1997**, *277*, 513. (c) Wolter,

K.; Seiferth, O.; Libuda, J.; Kuhlenbeck, H.; Bäumer, M.; Freund, H.-J. *Surf. Sci.* **1998**, *402*−404., 428. (d) Frank, M.; Bäumer, M.; Kühnemuth, R.; Freund, H.-J. *J. Phys. Chem. B* **2001**, *105*, 8569.

(36) Fukui, K.-I.; Aruga, T.; Iwasawa, Y. *Surf. Sci.* **1993**, *281*, 241.

(37) (a) Rodriguez, J. A. *Surf. Sci.* **1994**, *303*, 366. (b) Rodriguez, J. A. *Surf. Sci. Rep.* **1996**, *24*, 223. (c) Hammer, B.; Morikawa, Y.; Nørskov, J. K. *Phys. Rev. Lett.* **1996**, *76*, 2141.

(38) Rodriguez, J. A.; Dvorak, J.; Jirsak, T.; Hrbek, J. *Surf. Sci.* **2001**, *490*, 315.

(39) Song, Z.; Cai, T.; Rodriguez, J. A.; Hrbek, J.; Chan, A. S. Y.; Friend, C. M. *J. Phys. Chem. B* **2003**, *107*, 1036.

(40) Kalff, M.; Comsa, G.; Michely, T. *Phys. Rev. Lett.* **1998**, *81*, 1255.

(41) Liu, P.; Rodriguez, J. A.; Muckerman, J. T.; Hrbek, J. *Surf. Sci.* **2003**, *530*, L313

(42) Brenner, A.; Burwell, R. L. *J. Am. Chem. Soc.* **1975**, *97*, 2565.

(43) Williams, C. C.; Ekerdt, J. G. *J. Phys. Chem.* **1993**, *97*, 6843.

(44) Jackson, R. L.; Tyndall, G. W. *J. Appl. Phys.* **1988**, *64*, 2092.

(45) Berkó, A.; Solymosi, F. *J. Catal.* **1999**, *183*, 91.

(46) Van't Blik, H. F. J.; Van Zon, J. B. A. D.; Huizinga, T.; Vis, J. C.; Koningsberger, D. C.; Prins, R. *J. Am. Chem. Soc.* **1985**, *107*, 3139.

(47) (a) Van't Blik, H. F. J.; Van Zon, J. B. A. D.; Huizinga, T.; Vis, J. C.; Koningsberger, D. C.; Prins, R. *J. Phys. Chem.* **1983**, *87*, 2264. (b) Berkó, A.; Ménesi, G.; Solymosi, F. *J. Phys. Chem.* **1996**, *100*, 17732.

(48) (a) Berkó, A.; Solymosi, F. *Surf. Sci.* **1998**, *411*, L900. (b) Berkó, A.; Solymosi, F. *J. Phys. Chem. B* **2000**, *104*, 10215.

(49) (a) Zhdanov, V. P. *Surf. Sci.* **1984**, *137*, 515. (b) Fu, T.-Y.; Tsong, T. T. *Surf. Sci.* **1999**, *421*, 157.